Macular Functional and Morphological Changes in Intermediate Age-Related Maculopathy

Vincenzo Parisi, Lucia Ziccardi, Eliana Costanzo, Massimiliano Tedeschi, Lucilla Barbano, Daniela Manca, Antonio Di Renzo, Paola Giorno, Monica Varano, and Mariacristina Parravano

IRCCS - Fondazione Bietti, Rome, Italy

Correspondence: Lucia Ziccardi, IRCCS Fondazione Bietti, Via Livenza 1, 00198 Rome, Italy; lucia.ziccardi@fondazionebietti.it.

Received: January 8, 2020
Accepted: April 3, 2020
Published: May 12, 2020

Citation: Parisi V, Ziccardi L, Costanzo E, et al. Macular functional and morphological changes in intermediate age-related maculopathy. *Invest Ophthalmol Vis Sci.* 2020;61(5):11. https://doi.org/10.1167/iovs.61.5.11

Purpose. The purpose of this study was to evaluate macular preganglionic function and to verify its relationship with retinal and choroidal morphology in patients with intermediate age-related macular degeneration (iAMD) patients.

Methods. All included patients performed multifocal electroretinogram (mfERG) for investigating on macular function from the central 15° of foveal eccentricity, spectral domain optical coherence tomography (SD-OCT) for studying retinal structure, enhanced depth imaging OCT (EDI-OCT) for the measure of choroidal vascularity index (CVI), and OCT-angiography (OCTA) for the evaluation of vessel density (VD) in the superficial and deep capillary plexus, and choriocapillaris (CC) layer.

Results. Twenty-seven patients with iAMD and 20 age-matched control eyes were analyzed. Significantly ($P < 0.01$) delayed and reduced mfERG responses in the central 0 to 2.5°, paracentral 2.5 to 5°, and overall 0 to 5° areas, as well as increased CVI values in both foveal (1 mm centered to the fovea) and fovea + parafovea areas (3 mm centered to the fovea), increased foveal and parafoveal (annular area of 1–3 mm centered to the fovea) retinal pigment epithelium thickness, and volume and parafoveal outer retinal volume were found in iAMD eyes as compared to controls. Moreover, iAMD eyes showed significantly ($P < 0.01$) reduced foveal and parafoveal OCTA-VD values in the CC layer when compared to controls. In the iAMD group, not significant ($P > 0.01$) correlations were found between morphological and functional parameters.

Conclusions. Our findings support a dysfunction of photoreceptors and bipolar cells in both foveal and parafoveal areas in the presence of outer retina, CC, and choroidal structural changes, however, not significantly correlated. The observed enlargement of luminal choroidal area (measured by CVI) is possibly compensatory to CC vascular insufficiency.

Keywords: intermediate AMD, mfERG, SD-OCT, OCT angiography

Age-related macular degeneration (AMD) is a chronic, multifactorial, and progressive degenerative disease affecting the central vision of subjects 55 years old or older, most commonly seen in industrialized countries.[1–4] AMD includes a wide spectrum of clinical presentations, from early to intermediate until advanced forms up to geographic atrophy,[5–7] with various degree of visual acuity (VA) and central visual field impairment.[5,8]

An univocal comprehension of AMD pathogenic mechanisms is not globally reached and the role of the retinal and choroidal components is yet not fully understood.[9–27] About this matter, it would be useful to study in depth the early functional and morphological changes and their relationship.

Macular function in intermediate AMD (iAMD) has been assessed by multifocal electroretinogram (mfERG).[28] By recording bioelectrical responses from selective retinal areas enclosed between 0° and 20° from the fovea,[29,30] early dysfunction of the foveal, and the parafoveal preganglionic elements has been found at this stage.[15,29–39]

Regarding the macular morphology, several studies performed by using spectral domain-optical coherence tomography (SD-OCT), described that in the initial stages of AMD the peculiar anatomic retinal findings, consisting of drusen and reticular pseudodrusen (also known as subretinal drusenoid deposits [SDD]) are associated with morphological changes of the outer retinal layers (ORLs)[13] with variable degrees of inner retinal layer (IRL) thinning.[9–12] The advent of the enhanced depth image (EDI)-OCT and of the OCT-angiography (OCTA) allowed us to better explore the involvement of the choroid in initial AMD. Reduced choroidal thickness (CT) in the presence of SDD,[14,16–19] reduced choriocapillaris (CC) vessel density (VD)[21–25] and changes in choroidal vascular texture measured by choroidal vascularity index (CVI),[19–20] suggest that vascular supply impairment of the choroid and CC, combined to retinal abnormalities, could be involved in the pathogenesis of AMD.

Although the literature reported several evidences of photoreceptors and bipolar cells' dysfunction and of chori-

Copyright 2020 The Authors

This work is licensed under a Creative Commons Attribution-NonCommercial-NoDerivatives 4.0 International License.

Downloaded from iovs.arvojournals.org on 04/24/2024

oretinal ultrastructural impairment in iAMD, very few and not completely exhaustive information are available on the relationship between macular functional and morphological changes in iAMD.[15,36,37]

Therefore, we aimed to study either the function of the macular pre-ganglionic elements (by mfERG) and the chorioretinal morphology (by SD-OCT and OCTA) in patients with iAMD and to verify whether a relationship between functional and structural changes exists at this stage of the disease.

Methods

Subjects

In this observational, cohort case-control study, controls and patients with iAMD (corresponding to the Age-Related Eye Disease Study [AREDS] category 3, characterized by extensive [as measured by drusen area], intermediate [>63 µm, <125 µm] drusen, at least 1 large [>125 µm], or multiple soft intermediate drusen [≥63 µm, ≤125 µm])[7] were enrolled.

Inclusion criteria were: VA >0.1 logMAR with a refractive error equal or lower than ±2 diopters, measured as spherical equivalent, absence of moderate to dense corneal or lens opacities, refractive surgery, glaucoma or ocular hypertension, medical history of intraocular inflammation, of retinal detachment or laser treatment, of systemic diseases under medical treatment, of ocular trauma, or of intake of drug therapies with toxic effects on the macula (e.g. chloroquine and oxazepam). This research followed the tenets of the Declaration of Helsinki and the study was approved by local institutional review boards (IRCCS - Fondazione Bietti, Rome, Italy). Each patient signed an informed consent. All methods were performed in accordance with the relevant guidelines and regulations (see International Society for Clinical Electrophysiology of Vision [ISCEV] standard below for electrophysiology).

Functional Evaluation

Multifocal Electroretinogram Recordings. In control and iAMD eyes, mfERG was recorded according to the standard ISCEV[40] and to our previously published method.[31,35,41–43]

In all eyes, mfERGs were binocularly recorded after pupil dilation (1% tropicamide) to a diameter of 7 to 8 mm. The cornea was anesthetized with 1% dicaine. The mfERGs were recorded bipolarly between an active electrode (Dawson-Trick-Litzkow [DTL]) thread electrodes) referenced to the temples (Ag/AgCl electrode placed on the correspondent temporal side of the frontal lobe) under photopic conditions. A small Ag/AgCl skin ground electrode was placed at the center of the forehead. Interelectrode resistance was <5 KOhms.

Briefly, 61 scaled hexagons were displayed on a high-resolution, black-and-white monitor (size 30 cm width and 30 cm height) with a frame rate of 75 hertz (Hz). The array of hexagons subtended 20° of visual field. Each hexagon was independently alternated between black (1 cd/m^2) and white (200 cd/m^2) according to a binary m-sequence. Contrast was of 99%. The luminance of the monitor screen and the central fixation cross (used as target) was 100 cd/m^2. The m-sequence had 2^{13-1} elements and total recording time, divided into 8 segments, was approximately 4 minutes. Between segments, the subject was allowed to rest for a few seconds. Focusing lenses were used when necessary. Each patient, monitored by a video system in the screen of the computer, positively reported that he/she could clearly perceive the cross-fixation target.

The signal was amplified (gain 100,000) and filtered (band pass 1-100 Hz) by BM 6000 (Biomedica Mangoni, Pisa, Italy). After automatic rejection of artifacts (by VERIS Clinic version 4.9 software), the first order kernel response was examined.

We measured the time to peak (implicit time [IT]) of the first negative (N1) and the first positive (P1) peaks, and the averaged response amplitude densities (RADs) between the N1 and P1 peaks, obtained in four concentric annular retinal regions (rings = R) centered on the fovea. Therefore, we analyzed the N1 IT, P1 IT, and N1-P1 RADs derived from 0 to 2.5 (R1), from 2.5 to 5 (R2), from 5 to 10 (R3), from 10 to 15 (R4), and from 0–5 (R1 + R2) degrees.

The mfERGs were performed three times on three different days in each iAMD or control subject. The recording with the highest R1-R4 N1-P1 RAD was considered in the statistical analysis (see below).

Morphological Evaluation

SD-OCT Assessment. All subjects underwent structural SD-OCT scan using Heidelberg Spectralis (version 1.10.4.0; Heidelberg Engineering, Heidelberg, Germany) after pupil dilation. The SD-OCT imaging protocol consisted of at least 20° × 15° volume scans of the macula area with 19 B-scans. Furthermore, the EDI-OCT scans were acquired to better visualize the choroid.

All B-scan images were checked for errors in automatic segmentation and manual adjustments were used if uncorrected automatic segmentation occurred. Central macular thickness (CMT) and central macular volume (CMV), central inner retinal thickness (C-IRT), central inner retinal volume (C-IRV), central outer retinal thickness (C-ORT), central outer retinal volume (C-ORV), central retinal pigment epithelium thickness (C-RPE-T), and central retinal pigment epithelium volume (C-RPE-V) were automatically measured in the macular map centered to the fovea, through an inbuilt software of Heidelberg Spectralis (version 1.10.2.0). The IRL included the sum of inner plexiform layers (IPL) and innter nuclear layer (INL), whereas the ORL corresponded to the sum of outer plexiform layer (OPL) and the outer plexiform nuclear layer (ONL), whereas the retinal pigment epithelium (RPE) was automatically segmented by the device. The same parameters were measured in the parafoveal area (annular area 1–3 mm centered to the fovea): parafoveal macular thickness (P-MT) and parafoveal macular volume (P-MV), parafoveal inner retinal thickness (P-IRT), and parafoveal outer retinal thickness (P-ORT), parafoveal outer retinal volume (P-ORV), and parafoveal RPE thickness (P-RPE-T) and parafoveal RPE volume (P-RPE-V).

Two experienced operators (E.C. and M.T.) manually measured the CT in EDI-OCT scans, as the distance between hyper-reflective inferior limit of RPE and the hyper-reflective sclera-choroidal junction, using a caliper integrated into the device. Inter-observer agreement was calculated (Cohen's kappa 0.98 and 0.92), and measurements from the first operator (E.C.) were used for the study analysis. The CT was measured at the fovea (SCT), 1000 µm nasally (NCT), and 1000 µm temporally (TCT) to the fovea.

In the analysis of SD-OCT, we considered the following parameters: CMT (µm), CMV (mm^3), C-IRT (µm), C-IRV

Investigative Ophthalmology & Visual Science

Downloaded from iovs.arvojournals.org on 04/24/2024

(mm^3), C-ORT (µm), C-ORV (mm^3), C-RPE-T (µm), C-RPE-V (mm^3), P-MT (µm), P-MV (mm^3), P-IRT (µm), P-IRV (mm^3), P-ORT (µm), P-ORV (mm^3), P-RPE-T (µm), P-RPE-V (mm^3), SCT (µm), TCT (µm), and NCT (µm).

For the choroidal evaluation, the CVI has been calculated. CVI was obtained from the EDI-OCT scans, using a public domain software, ImageJ (version 1.49v https://imageJ.nih.gov/ij), as previously described by Sonoda et al.[44] Briefly, after a binarization using the Nidblack Autolocal Threshold Tool, we selected the fovea and parafovea choroidal regions, overlapping the ETDRS grid embedded in the Spectralis. Dark pixel corresponded to vascular lumen area (LA) and white pixel to stroma area (SA) in the selected region called total choroidal area (TCA). CVI was the ratio of the LA to the TCA. CVI was calculated in the foveal region (CVI-F, 1 mm centered to the fovea; i.e. 0.5 mm nasal and 0.5 temporal) and in the foveal plus parafoveal region (CVI-F + PF, 3 mm centered to the fovea; i.e. 1.5 nasal and 1.5 temporal).

OCTA Assessment. OCTA was performed using a commercially available AngioVue RTVue XR Avanti (Optovue, Fremont, CA, USA) beta version for clinical v.2018.1.0.33, that provides four automated segmented scans at the level of superficial capillary plexus (SCP), deep capillary plexus (DCP), avascular retina, and CC, using an algorithm called split-spectrum amplitude-decorrelation algorithm (SSADA).[45] The SCP: upper limit inner limiting membrane (ILM), lower limit 9 micron below the IPL; DCP: upper limit 9 micron below the IPL, lower limit 9 micron below the OPL; CC: upper limit 9 micron above the Bruch's membrane (BRM), and lower limit 31 micron below the BRM. The incorporated software algorithm SSADA generates 3-dimensional enface angiograms by the decorrelation of two merged consecutive orthogonal registration volumes automatically centered at the macula or manually centered at the lesion.

Each acquired OCTA volume (3 x 3 mm) consisted of 304 x 304 A-scan in 2.6 seconds. Each orthogonal volume registration is corrected to minimize motion artifacts. Both orthogonal volume scans are combined by a motion correction technology to create a 3-dimensional image of retinal and choroidal blood flow. A co-registered cross-sectional OCT B-scan allows the visualization of retinal structure. The OCTA software was used to manually adjust the automated segmentation and its relative depth in the retina and choroid. Patients with poor quality OCTA images (i.e. due to eye movement, motion artifacts, vitreous floaters, and/or Signal Strength Index (SSI) ≤50) were not included in the analysis. No images were excluded for incorrect position outside the fovea. An automated software, embedded in the instrument, calculated the VD at the level of SCP, DCP, and CC in the fovea and parafovea regions. The value of foveal avascular zone (FAZ) was also automatically extracted by the device.

Morpho-Functional Correlations

In order to evaluate a potential relationship between electro-functional abnormalities and retinal or choroidal morphological changes, we correlated mfERG parameters with SD-OCT and OCTA data derived from corresponding localized retinal areas.[46] To compare SD-OCT and OCTA results from almost superimposable circular foveal (1 mm), annular parafoveal (1–3 mm), and circular foveal plus parafoveal (3 mm) areas, we considered mfERG results from ring 1 (0–2.5°), ring 2 (2.5–5°), and ring 1 + ring 2 (0–5°), respectively.

Statistical Analysis

Sample size estimates were obtained from pilot evaluations of mfERG recordings performed in 10 patients with iAMD other than those included in the current study (unpublished results), using R1 RAD as the main outcome measure. It has been obtained that a number of 10 subjects for controls and iAMD groups, based on the following data: mean = 89.2 nV/deg^2, SD = 14.85 nV/deg^2 for controls and mean = 59.3 nV/deg^2, SD = 15.61 nV/deg^2 for patients with iAMD, that provided a power of 90% at an alpha = 0.01, to detect a between group difference of 33.52% in mfERG amplitude with reference to R1 RAD of controls. The Anderson–Darling and Kolmogorov–Smirnov tests were applied to verify that data were normally distributed. For all mfERG parameters, 95% normal confidence limits were obtained from age-similar normal subjects' data by calculating mean values minus 2 SD for RAD and mean values plus 2 SD for IT. Only one eye was chosen for each patient with iAMD or control subject. Differences of mfERG, OCT, and OCT-A values between controls and iAMD groups were evaluated by the 1-way ANOVA. Linear correlations between mfERG and morphological changes were assessed by Pearson's test. All statistical analyses were performed using SPSS version 26 (Statistical Package for Social Science IBM), and a P value < 0.01 was considered as statistically significant.

Results

Twenty-seven eyes following the diagnostic criteria of iAMD[7] from 27 patients (18 women and 9 men, mean age 69.3 ± 9.2 years) were enrolled in the study (iAMD group). Patients were selected on the basis of inclusion criteria (see above) from a larger cohort of 82 patients with AMD. A group of 20 age-matched healthy subjects (13 women and 7 men, mean age: 70.02 ± 8.7 years), providing 20 normal eyes, served as controls. When both eyes fulfilled the inclusion criteria, the eye with the best VA was selected; when both eyes had the same VA, the right eye was chosen for analysis.

Functional (mfERG) Data

Figure 1A shows the 61 hexagons trace arrays subtending 15° of visual field for control and iAMD representative eyes, where it could be qualitatively observed a not symmetrical radial dysfunction, as for the topographical localization of drusen. Figure 1B shows mfERG traces recorded from one control eye and from two iAMD eyes (iAMD #7 and iAMD #18). R1, R2, and R1 + R2 N1 IT, P1 IT, and N1-P1 RADs were significantly (P < 0.01) delayed and reduced in iAMD eyes when compared to control eyes. In the more external rings (R3–R4), not significant (P > 0.01) differences between iAMD and control groups were found for all mfERG parameters.

Mean values and relative statistical analysis of mfERG parameters are reported in Table 1.

Morphological (SD-OCT and OCTA) Data

Examples of SD-OCT, EDI-OCT, and OCTA scans from one control eye and two iAMD eyes (iAMD #7 and iAMD #18) are presented in Figure 2.

Mean values of SD-OCT and EDI-OCT parameters (CMT, CMV, C-IRT, C-IRV, C-ORT, C-ORV, P-MT, P-MV, P-IRT, P-IRV, P-ORT, SCT, TCT, and NCT) were not significantly (P > 0.01)

Investigative Ophthalmology & Visual Science

Downloaded from iovs.arvojournals.org on 04/24/2024

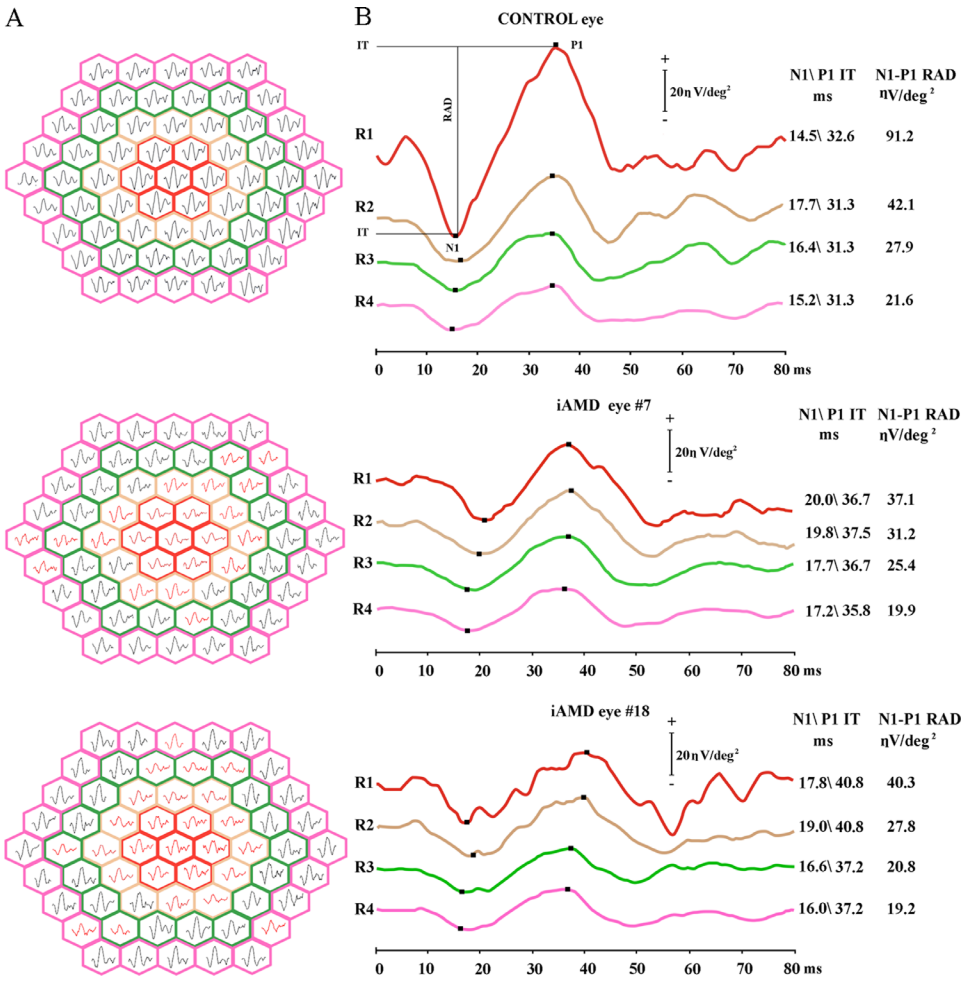

Figure 1. (A) Multifocal electroretinogram (mfERG) bioelectrical responses obtained from 15° of foveal eccentricities in one control eye and in two representative eyes affected by intermediate age-related macular degeneration (iAMD #7 and iAMD #18). In iAMD #7 and iAMD #18 eyes, we depicted in black the mfERG traces whose response amplitude density and implicit time were within normal limits, and in red the mfERGs with delayed implicit time and/or reduced response amplitude density. (B) Examples of mfERG responses recorded from four averaged annular areas (rings = R) with increasing eccentricity from the fovea to the retinal mid-periphery: 0 to 2.5 (R1), 2.5 to 5 (R2), 5 to 10 (R3), and 10 to 15 (R4) degrees in one control eye and iAMD #7 and iAMD #18 that showed, with respect to the control eye, an increase in N1 and P1 implicit time (IT) and a decrease in N1-P1 response amplitude density (RAD) exclusively in the most central macular areas (R1 and R2). In the more peripheral retinal areas (R3-R4), mfERG responses (N1 and P1 IT and N1-P1 RAD) were similar between iAMD eyes and control eyes.

different between control and iAMD groups. Mean values of central and parafoveal RPE-T, RPE-V, and P-ORV detected in the iAMD group were significantly ($P < 0.01$) increased compared to controls.

The CVI values were significantly increased ($P < 0.01$) in iAMD eyes compared to those of controls in both foveal (1 mm centered on the fovea) and fovea + parafovea areas (3 mm centered on the fovea).

The analysis of VD, obtained from OCTA layers, showed not significant ($P > 0.01$) differences in SCP and DCP between the iAMD and control groups, whereas a significant ($P < 0.01$) reduction of CC VD (both foveal and parafoveal) was detected in the iAMD group when compared to the control group. FAZ was not significantly different ($P > 0.01$) between groups.

Mean values and relative statistical analysis between the iAMD and control groups of SD-OCT and OCTA parameters are reported in Table 2 and Table 3, respectively.

Correlations Between Functional and Morphological Data

When in iAMD eyes the values of mfERG parameters were correlated to SD-OCT, EDI-OCT, and OCTA data from corresponding macular areas, not significant ($P > 0.01$) correlations were found. These data are presented in Table 4.

Discussion

Our study aimed to evaluate the function of macular preganglionic elements (by mfERG recordings) as well as the retinal and choroidal structure (by SD-OCT and OCTA assessment) in iAMD, and to verify whether a relationship between function and morphology exists at this stage of the degenerative disorder.

Macular function of iAMD eyes was impaired as compared to controls, only in the foveal and parafoveal

Investigative Ophthalmology & Visual Science

Downloaded from iovs.arvojournals.org on 04/24/2024

Table 1. Mean Values ± 1 SD of mfERG N1 and P1 ITs and N1-P1 RADs Observed in Control Eyes (C; 20 Eyes) and iAMD Eyes; 27 Eyes) Groups

	mfERG		ANOVA Versus Control	
	Mean	**SD**	**F (1, 46)**	***P***
R1 N1 IT, msec				
C	13.83	2.58		
iAMD	16.30	2.60	9.09	**0.005**
R1 P1 IT, msec				
C	30.26	1.55		
iAMD	38.80	5.81	40.84	**<0.001**
R1 RAD, nanoV/degree^2				
C	83.32	13.82		
iAMD	56.61	14.15	41.75	**<0.001**
R2 N1 IT, msec				
C	17.22	2.72		
iAMD	20.53	2.61	17.83	**<0.001**
R2 P1 IT, msec				
C	30.82	1.47		
iAMD	37.21	4.40	38.78	**<0.001**
R2 RAD, nanoV/degree^2				
C	39.22	5.62		
iAMD	26.50	6.41	50.14.	**<0.001**
R1 + R2 N1 IT, msec				
C	15.12	2.64		
iAMD	20.58	2.99	42.24	**<0.001**
R1+R2 P1 IT, msec				
C	32.42	2.87		
iAMD	36.22	2.43	24.08	**<0.001**
R1 + R2 RAD, nanoV/degree^2				
C	36.76	5.88		
iAMD	23.47	8.41	36.59	**<0.001**
R3 N1 IT, msec				
C	18.64	2.32		
iAMD	19.09	2.82	0.34	0.536
R3 P1 IT, msec				
C	34.22	2.47		
iAMD	36.13	4.32	3.14	0.083
R3 RAD, nanoV/degree^2				
C	17.23	2.93		
iAMD	15.41	4.14	2.81	0.100
R4 N1 IT, msec				
C	18.32	3.21		
iAMD	18.43	2.37	0.02	0.893
R4 P1 IT, msec				
C	33.87	2.96		
iAMD	34.73	3.21	0.88	0.353
R4 RAD, nanoV/degree^2				
C	13.14	3.72		
iAMD	12.70	3.32	0.18	0.672

The mfERG responses were recorded from four averaged annular areas (rings = R) with increasing eccentricity from the fovea to the retinal mid-periphery: 0 to 2.5 (R1), 2.5 to 5 (R2), 0 to 5 (R1 + R2), 5 to 10 (R3), and 10 to 15 (R4) degrees. Statistics: 1-way ANOVA between control and iAMD groups.

areas, as reduced mfERG N1-P1 RADs and delayed N1 and P1 ITs were found only in the 0 to 2.5° (R1) and 2.5 to 5° (R2). Because the mfERG first order kernel responses originate from photoreceptors and off bipolar cells,[29] our findings suggest dysfunction of cone-mediated central pre-ganglionic elements in iAMD, in addition to the already reported rod impairment.[34] These evidences agree with previous description of either N1-P1 RAD decrease and N1 IT delay in the foveal and parafoveal areas in precocious stages of AMD (early and iAMD)[28,39] as well as in asymptomatic fellow eyes.[32] Contrary to our finding of P1 IT delay, Yavas et al.[39] described that this parameter could be altered in more advanced phases of the disease (late AMD). We did not find any significant mfERG changes in the more peripheral retinal areas (5–15°), unlike other authors[28] who reported abnormal mfERG responses up to 20° of foveal eccentricity in a more heterogeneous group of dry and wet AMD.

The first pathophysiologic mechanisms at the basis of AMD are the extracellular macular deposition under the RPE of waste products forming drusen and the accumulation of phospholipids in the inner collagen layer of BRM.[47] The excessive accumulation of lipofuscin in RPE cells, which is greatest under the parafoveal retina,[48,49] as well as the mechanical displacement of the photoreceptors' outer segments and/or a defect of the nutrient exchange between photoreceptors and CC for the deposition of soft drusen under the RPE, has been reported in aged retinas.[50–52] Therefore, it is likely that the observed outer retina dysfunction may be associated with mechanical and metabolic abnormalities.

Regarding the retinal morphology, significant differences in foveal and parafoveal RPE thickness and volume (C-RPE-T, C-RPE-V, P-RPE-T, and P-RPE-V) and P-ORV measured by SD-OCT were found in iAMD eyes compared with controls. For instance, according to previous studies,[11,53,54] we found significant RPE thickening in iAMD eyes, whereas mean CMT, CMV, P-MT, P-MV, and the foveal and parafoveal inner and outer retina thickness (C-IRT, C-ORT, P-IRT, and P-ORT) values were similar in both groups. The absence of thickness abnormalities of inner and outer retina at this stage of the disease, with VA preservation, has been reported mostly when using CMT as main parameter of evaluation.[9,10,12,15] However, contrasting data were found when analyzing focal areas. For example, Nusinowitz et al.[12] found nonsignificant thinning of total retina in early AMD, but thickening of the outer retina in the paradrusen area. This data was previously reported also by Sadigh et al.,[55] who found a variable thickness of the outer retina in early and iAMD. Recently, Lamin at al.[11] analyzed a population of patients with early and intermediate AMD, describing an increase of RPE-BRM complex volume associated with an increase in OPL and ONL volume in the central macular area of 6 mm diameter. Our data are in agreement with these observations concerning the analysis of RPE thickness and volume that increased in foveal and parafoveal areas (0-3 mm) in iAMD versus controls. This could be due to the accumulation of lipofuscin in RPE cells,[48,49] hypothesizing that it is dependent to the mechanism of drusen formation.[11] Regarding macular volume, our analysis of P-ORV confirmed the increase in ORL volume in iAMD previously reported by Lamin et al.,[11] who also supposed an expansion in OPL due to a displacement of nuclei from ONL to OPL.

In iAMD eyes, the ultra-structural analysis of the choroid that we obtained by measuring the CT at the level of the fovea and 1000 µm nasally (NCT) and temporally away from the fovea (TCT) showed not significant differences in the two groups. Similar or contrasting results were found using the same parameter by EDI-OCT in the initial stages of AMD.[14,16–19] However, we added to the conventional study of the choroid a novel parameter, known as CVI, representing the ratio between the luminal area and the total choroidal area in a selected region.[44] A significant increase of CVI in both the foveal and parafoveal regions was found in our iAMD eyes when compared to control eyes. This finding can be due to a potential vasodilation process expressed as an

Investigative Ophthalmology & Visual Science

Downloaded from iovs.arvojournals.org on 04/24/2024

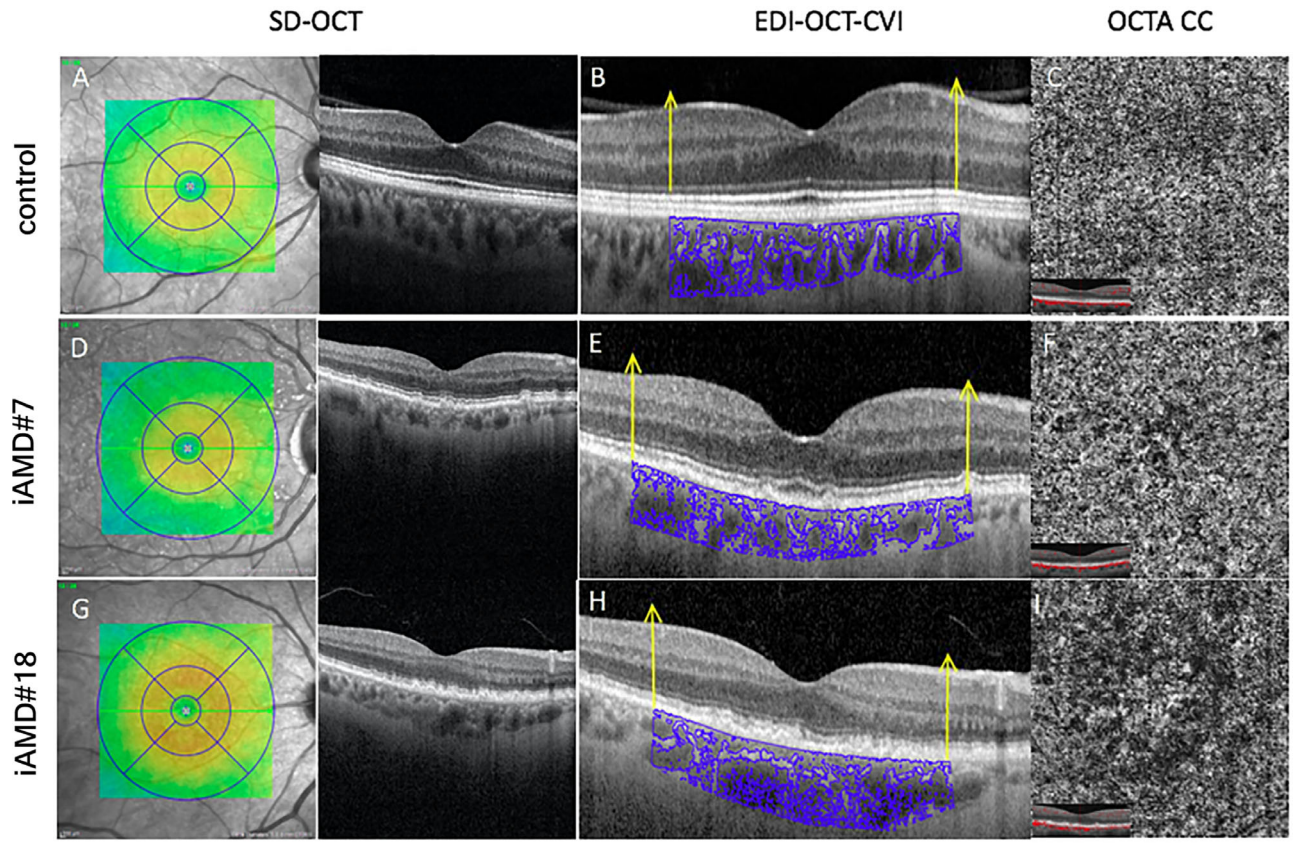

Figure 2. Multimodal morphological imaging recorded in one control eye (upper row) and in two representative eyes affected by intermediate age-related macular degeneration (iAMD #7 and iAMD #18) (middle and bottom row). Spectral domain-optical coherence tomography (SD-OCT). (A, D, G) Enhanced depth imaging-OCT (B, E, H), and OCT angiography (OCTA), (C, F, I) 3 × 3 scans imaged by AngioVue. In iAMD eyes, SD-OCT scans showed drusen and reticular pseudo-drusen (D, G), choroidal vascularity index (CVI) analysis showed an increase in parafoveal area (marked with yellow arrows), (E, H) and CC OCTA scan showed a vessel density reduction in iAMD eyes (F, I) compared with control eyes (C). SD-OCT images have different magnification rate compared to EDI-OCT images, due to the technique used for CVI calculation that needs to crop the EDI-OCT using ImageJ.

increase in luminal vessel area at the choroid level that may occur in iAMD eyes. Our results are supported by Keenan et al.,[19] who studied the choroidal blood supply by means of CVI, detecting an increase of this parameter in the initial stage of AMD; the presence of drusen alone has also been correlated with an increase of CVI.[18,19]

To better understand whether the increase of CVI could be expression of potential choroidal compensatory effect, we studied the possible CC changes by OCTA evaluation. Using the automatically extracted parameters (by the device), our iAMD eyes showed a significant reduction in VD of CC layer (in the foveal and parafoveal areas) without other significant changes of retinal vascular parameters (SCP and DCP layers, as well as FAZ). This finding could result from a vascular flow impairment associated to drusenoid deposits that characterize the initial stages of AMD. Similar insufficiency of the CC, identified by decreased CC VD,[22–27,50] as well as deficiency of vascular supply in retinal layers (detected by reduced VD in SCP and DCP[22,24]) that, however, we did not confirm, has been reported in previous OCTA studies.[22–27] Our results support the hypothesis, also suggested by Keenan et al.,[19] that an increase of choroidal blood supply could occur to compensate deficiency of the CC vascular flow in iAMD.

With respect to the aim of the study, our findings led us to hypothesize that reduced CC VD flow may produce hypoxia (for the low oxygen delivery) and can impair the oxidative metabolism driving phototransduction (leading to RPE and photoreceptor failure[56]). These vascular changes together with mechanical and metabolic abnormalities can induce dysfunction of the foveal and parafoveal pre-ganglionic elements in iAMD. A possible compensatory mechanism to this choriocapillaris vascular insufficiency, as already supposed,[19] could determine choroidal vasodilation and a relative increase of choroidal luminal area. No significant correlations between functional and retino-choroidal morphological parameters were detected in patients with iAMD. We are aware that few and discordant studies investigated on the correlation between functional and morphological parameters, however, without matching all parameters from almost corresponding areas. For instance, Garcia-Garcia et al.[37] found delayed N1 and P1 ITs, with not significant correlations between central retinal thickness and macular function in 10 patients with drusen maculopathy. In addition, Gerth et al.[30] showed cone-driven pathway dysfunction, especially related to ITs, not correlated to retinal morphological changes, consisting of large drusen. In early and iAMD eyes, Yang et al.[15] found statistically significant correlations between reduced N1-P1 RADs and decreased retinal photoreceptor thickness within 3 mm from the foveola and, more recently, Borrelli et al.[56] described a correlation between CC perfusion dropout and macular

Downloaded from iovs.arvojournals.org on 04/24/2024

Table 2. Mean values ± 1 SD of SD-OCT Parameters Observed in Control (C; 20 Eyes) and iAMD (27 Eyes) Groups.

	SD-OCT		ANOVA Versus Control	
	Mean	**SD**	**F (1, 46)**	***P***
CMT, µm				
C	277.10	16.52		
iAMD	278.00	22.71	0.02	0.881
CMV, mm³				
C	0.22	0.01		
iAMD	0.22	0.01	0.00	1.000
C-IRT, µm				
C	41.70	6.62		
iAMD	41.48	6.76	0.01	0.912
C-IRV, mm³				
C	0.03	0.08		
iAMD	0.03	0.01	0.00	1.000
C-ORT, µm				
C	120.20	5.55		
iAMD	119.00	16.24	0.10	0.753
C-ORV, mm³				
C	0.09	0.05		
iAMD	0.09	0.01	0.80	1.000
C-RPE-T, µm				
C	15.09	1.52		
iAMD	21.11	6.18	13.53	**<0.001**
C-RPE-V, mm³				
C	0.009	0.001		
iAMD	0.016	0.006	26.53	**<0.001**
SCT, µm				
C	245.00	59.10		
iAMD	228.07	46.36	1.21	0.277
TCT, µm				
C	242.30	55.10		
iAMD	238.11	50.52	0.07	0.788
NCT, µm				
C	235.50	72.20		
iAMD	228.59	54.31	0.14	0.710
CVI-F				
C	0.66	0.02		
iAMD	0.70	0.05	11.39	**0.002**
CVI-F + PF				
C	0.67	0.03		
iAMD	0.71	0.04	14.09	**<0.001**
P-MT, µm				
C	340.21	13.61		
iAMD	334.03	14.12	2.27	0.139
P-MV, mm³				
C	0.53	0,02		
iAMD	0.52	0,02	2.87	0.097
P-IRT, µm				
C	82.67	4.82		
iAMD	80.23	4.48	3.20	0.081
P-IRV, mm³				
C	0.13	0.01		
iAMD	0.12	0.02	4.20	0.046
P-ORT, µm				
C	102.21	4.33		
iAMD	109.42	30.03	1.13	0.294
P-ORV, mm³				
C	0.15	0.01		
iAMD	0.17	0.02	16.81	**<0.001**
P-RPE-T, µm				
C	15.88	1.16		
iAMD	18.02	3.32	7.59	**0.008**
P-RPE-V, mm³				
C	0.02	0.003		
iAMD	0.03	0.007	35.78	**<0.001**

Statistics: 1-way ANOVA between controls and iAMD groups.

CMT, central macular thickness; CMV, central macular volume; C-IRT, central inner retinal thickness; C-IRV, central inner retinal volume; C-ORT, central outer retinal thickness; C-ORV, central outer retinal volume; C-RPE-T, central retinal pigment epithelium thickness; C-RPE-V, central retinal pigment epithelium volume; SCT, subfoveal choroidal thickness; TCT, temporal choroidal thickness; NCT, nasal choroidal thickness; CVI, choroidal vascularity index; CVI-F, choroidal vascularity index fovea (1 mm centered on the fovea); CVI-F + PF, choroidal vascularity index fovea + parafovea (3 mm centered on the fovea); P-MT, parafoveal macular thickness; P-MV, parafoveal macular volume; P-IRT, parafoveal inner retinal thickness; P-IRV, parafoveal inner retinal volume; P-ORT, parafoveal outer retinal thickness; P-ORV, parafoveal outer retinal volume; P-RPE-T, parafoveal retinal pigment epithelium thickness; P-RPE-V, parafoveal retinal pigment epithelium volume.

Table 3. Mean Values ± 1 SD of OCTA Parameters Observed in Control (C; 20 Eyes) and iAMD (27 Eyes) Groups

	OCTA		ANOVA Versus Control	
	Mean	**SD**	**F (1, 46)**	***P***
FAZ				
C	0.22	0.10		
iAMD	0.26	0.09	2.06	0.158
VD-SCP-F				
C	23.40	4.73		
iAMD	24.24	6.64	0.23	0.632
VD-SCP-P				
C	46.52	3.22		
iAMD	47.36	3.88	0.62	0.435
VD-DCP-F				
C	33.92	6.36		
iAMD	34.17	5.69	0.02	0.888
VD-DCP-P				
C	48.89	4.84		
iAMD	48.89	4.02	0.00	1.000
VD-CC-F				
C	70.66	5.57		
iAMD	56.08	15.45	16.17	**<0.001**
VD-CC-P				
C	68.62	4.37		
iAMD	61.89	8.99	9.50	**0.003**

Statistics: 1-way ANOVA between control and iAMD groups.

FAZ, fovea avascular zone; VD, vessel density; SCP, superficial capillary plexus; DCP, deep capillary plexus; CC, choriocapillaris; F, fovea (foveal area automatically extracted by the device); P, parafovea (parafoveal area automatically extracted by the device).

function studying 17 patients with iAMD. Specifically, an increase of parafoveal percent nonperfused CC area was found significantly correlated with mfERG N1 IT delay in R2 area, thus suggesting an association between dysfunctional photoreceptors' mediated pathway and CC. In our study, however, we were not able to confirm these evidences, due to different reasons. The first reason is that CC VD was automatically extracted by the device, as a different OCTA parameter to study the CC integrity. Another reason is the inability of this technique to remove the shadowing effect

Investigative Ophthalmology & Visual Science

Downloaded from iovs.arvojournals.org on 04/24/2024

Downloaded from iovs.arvojournals.org on 04/24/2024

Table 4. Correlations (Pearson's test) Between mfERG Values Detected in the Foveal, Parafoveal, and Foveal + Parafoveal Areas (R1: 0–2.5, R2: 2.5–5, and R1+R2:0–5 Degrees) and Values of SD-OCT and OCTA Parameters Measured in Almost Corresponding Retinal Areas in iAMD Eyes

	Correlation With					
SD-OCT Parameters	**mfERG R1N1 IT (R = ; *P* =)**	**mfERG R1P1 IT (R = ; *P* =)**	**mfERG R1RAD (R = ; *P* =)**	**mfERG R2N1 IT (R = ; *P* =)**	**mfERG R2P1 IT (R = ; *P* =)**	**mfERG R2RAD (R = ; *P* =)**
CMT	0.066; 0.740	−0.203; 0.319	0.01; 0.968	–	–	–
PMT				0.219; 0.270	0.096; 0.631	−0.018; 0.962
CMV	0.008; 0.965	−0.276; 0.172	0.124; 0.536	–	–	–
PMV				0.206; 0.302	0.105; 0.602	−0.002; 0.989
C-IRT	0.245; 0.271	0.195; 0.340	−0.044; 0.831	–	–	–
P-IRT				−0.363; 0.062	−0.161; 0.419	0.029; 0.884
C-IRV	−0.061; 0.759	0.182; 0.373	−0.01; 0.962	–	–	–
P-IRV				0.103; 0.606	−0.155; 0.439	0.281; 0.154
C-ORT	−0.180; 0.368	−0.156; 0.447	0.189; 0.344	–	–	–
P-ORT				0.252; 0.203	0.355; 0.032	0.095; 0.635
C-ORV	−0.163; 0.414	0.014; 0.942	0.09; 0.649	–	–	–
P-ORV				0.270; 0.172	0.050; 0.801	−0.197; 0.324
C-RPE-T	0.134; 0.505	−0.329; 0.096	0.176; 0.378	–	–	–
P-RPE-T				0.123; 0.539	0.080; 0.689	0.356; 0.067
C-RPE-V	0.088; 0.661	−0.292; 0.138	0.109; 0.587	–	–	–
P-RPE-V				0.131; 0.512	0.181, 0.364	0.316; 0.107
SCT	−0.369; 0.067	−0.370; 0.060	0.300; 0.128	–	–	–
CVI-F	−0.211; 0.290	−0.224; 0.260	0.136; 0.496	–	–	–
TCT	–	–	–	−0.343; 0.079	−0.175; 0.392	0.306; 0.067
NCT	–	–	–	−0.362; 0.088	−0.294; 0.144	0.311; 0.122
				mfERG R1+R2 N1 IT (R = ; *P* =)	**mfERG R1+R2 P1 IT (R = ; *P* =)**	**mfERG R1+R2 RAD (R = ; *P* =)**
CVI-F+PF	–	–	–	−0.214; 0.281	−0.034; 0.866	0.375; 0.025

	Correlation With					
OCTA Parameters	**mfERG R1 N1 IT (R = ; *P* =)**	**mfERG R1 P1 IT (R = ; *P* =)**	**mfERG R1 RAD (R = ; *P* =)**	**mfERG R2 N1 IT(R = ; *P* =)**	**mfERG R2 P1 IT (R = ; *P* =)**	**mfERG R2 RAD (R = ; *P* =)**
FAZ	−0.036; 0.857	0.288; 0.144	0.161; 0.419	–	–	–
VD-SCP-F	0.229; 0.249	−0.316; 0.108	−0.248; 0.211	–	–	–
VD-SCP-P	–	–	–	0.054; 0.787	0.241; 0.224	0.107; 0.593
VD-DCP-F	−0.094; 0.637	−0.250; 0.207	−0.36; 0.064	–	–	–
VD-DCP-P	–	–	–	−0.091; 0.650	0.098; 0.626	0.148; 0.460
VD-CC-F	−0.264; 0.182	0.213; 0.284	0.130; 0.516	–	–	–
VD-CC-P	–	–	–	0.041; 0.839	-0.180, 0.367	0.327; 0.095

IT, implicit time; RAD, response amplitude density; CMT, central macular thickness; CMV, central macular volume; C-IRT, central inner retinal thickness; C-IRV, central inner retinal volume; C-ORT, central outer retinal thickness; C-ORV, central outer retinal volume; C-RPE-T, central retinal pigment epithelium thickness; C-RPE-V, central retinal pigment epithelium volume; SCT, subfoveal choroidal thickness; TCT, temporal choroidal thickness; NCT, nasal choroidal thickness; P-MT, parafoveal macular thickness; P-MV, parafoveal macular volume; P-IRT, parafoveal inner retinal thickness; P-IRV, parafoveal inner retinal volume; P-ORT, parafoveal outer retinal thickness; P-ORV, parafoveal outer retinal volume; P-RPE-T, parafoveal retinal pigment epithelium thickness; P-RPE-V, parafoveal retinal pigment epithelium volume; CVI, choroidal vascularity index; CVI-F, choroidal vascularity index-fovea (1 mm centered on the fovea); CVI-F+PF, choroidal vascularity index fovea + parafovea (3 mm centered on the fovea); FAZ, fovea avascular zone; VD, vessel density; SCP, superficial capillary plexus; DCP, deep capillary plexus; CC, choriocapillaris; F, fovea; P, parafovea.

of drusen on the CC slab, which represents one of the critical debated points in the CC analysis.

In conclusion, in our patients with iAMD, the multimodal analysis with innovative and noninvasive techniques was helpful to detect a dysfunction of photoreceptors and bipolar cells in both foveal and parafoveal areas in the presence of the outer retina, choriocapillaris, and choroidal changes, however, not significantly correlated. By adding the analysis of the luminal choroidal area (CVI), we hypothesized a choroidal compensatory phenomenon to the CC insufficiency. Our findings, remarking a key role of choroid in iAMD pathogenesis, encourage further investigations on this topic.

Acknowledgments

The authors thank Valter Valli Fiore for his technical assistance in the electrophysiological evaluations and Maria Luisa Alessi for graphical assistance.

The contribution of IRCCS- Fondazione Bietti was supported by the Italian Ministry of Health and Fondazione Roma. The authors alone are responsible for the content and writing of the paper.

Disclosure: **V. Parisi,** None; **L. Ziccardi,** None; **E. Costanzo,** None; **M. Tedeschi,** None; **L. Barbano,** None; **D. Manca,** None; **A. Di Renzo,** None; **P. Giorno,** None; **M. Varano,** None; **M. Parravano,** None

References

1. Klein R, Klein BE, Knudtson MD, Meuer SM, Swift M, Gangnon RE. Fifteen-year cumulative incidence of age-related macular degeneration: The Beaver Dam Eye Study. *Ophthalmology*. 2007;114:253–262.
2. Bressler NM, Bressler SB, Fine SL. Age-related macular degeneration. *Surv Ophthalmol*. 1988;32:375–413.
3. Resnikoff S, Pascolini D, Etya'ale D, et al. Global data on visual impairment in the year 2002. *Bull World Health Organ*. 2004;82:844–885.
4. Evans JR, Fletcher AE, Wormald RP, et al. Prevalence of visual impairment in people aged 75 years and older in Britain: results from the MRC trial of assessment and management of older people in the community. *Br J Ophthalmol*. 2002;86:795–800.
5. Graham KW, Chakravarthy U, Hogg RE, Muldrew KA, Young IS, Kee F. Identifying features of early and late age-related macular degeneration: a comparison of multicolor versus traditional color fundus photography. *Retina*. 2018;38:1751–1758.
6. Steinberg JS, Gobel AP, Fleckenstein M, Holz FG, Schmitz-Valckenberg S. Reticular drusen in eyes with high-risk characteristics for progression to late-stage age-related macular degeneration. *Br J Ophthalmol*. 2015;99:1289–1294.
7. Ferris FL, Wilkinson CP, Bird A, et al. Beckman Initiative for Macular Research Classification Committee. Clinical classification of age-related macular degeneration. *Ophthalmology*. 2013;120:844–851.
8. Steinberg JS, Fleckenstein M, Holz FG, Schmitz-Valckenberg S. Foveal sparing of reticular drusen in eyes with early and intermediate age-related macular degeneration. *Invest Ophthalmol Vis Sci*. 2015;56:4267–4274.
9. Rimayanti U, Kiuchi Y, Yamane K, et al. Inner retinal layer comparisons of eyes with exudative age-related macular degeneration and eyes with age-related macular degeneration and glaucoma. *Graefes Arch Clin Exp Ophthalmol*. 2014;252:563–557.
10. Lee EK, Yu HG. Ganglion cell-inner plexiform layer and peripapillary retinal nerve fiber layer thicknesses in age-related macular degeneration. *Invest Ophthalmol Vis Sci*. 2015;56:3976–3983.
11. Lamin A, Oakley JD, Dubis AM, Russakoff DB, Sivaprasad S. Changes in volume of various retinal layers over time in early and intermediate age-related macular degeneration. *Eye (Lond)*. 2019;33:428–434.
12. Nusinowitz S, Wang Y, Kim P, et al. Retinal structure in pre-clinical age-related macular degeneration. *Curr Eye Res*. 2018;43:376–382.
13. Schuman SG, Koreishi AF, Farsiu S, Jung SH, Izatt JA, Toth CA. Photoreceptor layer thinning over drusen in eyes with age-related macular degeneration imaged in vivo with spectral-domain optical coherence tomography. *Ophthalmology*. 2009;116:488–496.
14. Yiu G, Chiu SJ, Petrou P, et al. Relationship of central choroidal thickness with age-related macular degeneration status. *Am J Ophthalmol*. 2015;159:617–626.
15. Yang S, Zuo C, Xiao H, et al. Photoreceptor dysfunction in early and intermediate age-related macular degeneration assessed with mfERG and spectral domain OCT. *Doc Ophthalmol*. 2016;132:17–26.
16. Capuano V, Souied EH, Miere A, Jung C, Costanzo E, Querques G. Choroidal maps in non-exudative age-related macular degeneration. *Br J Ophthalmol*. 2016;100:677–682.
17. Laíns I, Wang J, Providência J, et al. Choroidal changes associated with subretinal drusenoid deposits in age-related macular degeneration using swept-source optical coherence tomography. *Am J Ophthalmol*. 2017;180:55–63.
18. Corvi F, Souied EH, Capuano V, et al. Choroidal structure in eyes with drusen and reticular pseudodrusen determined by binarisation of optical coherence tomographic images. *Br J Ophthalmol*. 2017;101:348–352.
19. Keenan TD, Klein B, Agrón E, Chew EY, Cukras CA, Wong WT. Choroidal thickness and vascularity vary with disease severity and subretinal drusenoid deposit presence in non advanced age-related macular degeneration. *Retina*. 2019;40:632–642.
20. Wei X, Ting DSW, Ng WY, Khandelwal N, Agrawal R, Cheung CMG. Choroidal vascularity index: a novel optical coherence tomography based parameter in patients with exudative age-related macular degeneration. *Retina*. 2017;37:1120–1125.
21. Esmaeelpour M, Ansari-Shahrezaei S, Glittenberg C, et al. Choroid, Haller's, and Sattler's layer thickness in intermediate age-related macular degeneration with and without fellow neovascular eyes. *Invest Ophthalmol Vis Sci*. 2014;55:5074–5080.
22. Toto L, Borrelli E, Mastropasqua R, et al. Association between outer retinal alterations and microvascular changes in intermediate stage age-related macular degeneration: an optical coherence tomography angiography study. *Br J Ophthalmol*. 2017;101:774–779.
23. Waheed NK, Moult EM, Fujimoto JG, Rosenfeld PJ. Optical coherence tomography angiography of dry age-related macular degeneration. *Dev Ophthalmol*. 2016;56:91–100.
24. Toto L, Borrelli E, Di Antonio L, Carpineto P, Mastropasqua R. Retinal vascular plexuses' changes in dry age-related macular degeneration, evaluated by means of optical coherence tomography angiography. *Retina*. 2016;36:1566–1572.
25. Borrelli E, Shi J, Uji A, et al. Topographic analysis of the choriocapillaris in intermediate age-related macular degeneration. *Am J Ophthalmol*. 2018;196:34–43.
26. Ahn SM, Lee SY, Hwang SY, Kim SW, Oh J, Yun C. Retinal vascular flow and choroidal thickness in eyes with early age-related macular degeneration with reticular pseudodrusen. *BMC Ophthalmol*. 2018;18:184.

Downloaded from iovs.arvojournals.org on 04/24/2024

27. Chatziralli I, Theodossiadis G, Panagiotidis D, Pousoulidi P, Theodossiadis P. Choriocapillaris' alterations in the presence of reticular pseudodrusen compared to drusen: study based on OCTA findings. *Int Ophthalmol*. 2018;38:1887–1893.
28. Huang S, Wu D, Jiang F, et al. The multifocal electroretinogram in age-related maculopathies. *Doc Ophthalmol*. 2000;101:115–124.
29. Hood DC. Assessing retinal function with the multifocal technique. *Prog Retin Eye Res*. 2000;19:607–646.
30. Gerth C, Delahunt PB, Alam S, Morse LS, Werner JS. Cone-mediated multifocal electroretinogram in age-related macular degeneration: progression over a long-term follow- up. *Arch Ophthalmol*. 2006;12:345–352.
31. Parisi V, Perillo L, Tedeschi M, et al. Macular function in eyes with early age-related macular degeneration with or without contralateral late age-related macular degeneration. *Retina*. 2007;27:879–890.
32. Li J, Tso MO, Lam TT. Reduced amplitude and delayed latency in foveal response of multifocal electroretinogram in early age related macular degeneration. *Br J Ophthalmol*. 2001;85:287–290.
33. Heinemann-Vernaleken B, Palmowski AM, Allgayer R, Ruprecht KW. Comparison of different high resolution multifocal electroretinogram recordings in patients with age- related maculopathy. *Graefes Arch Clin Exp Ophthalmol*. 2001;239:556–561.
34. Chen C, Wu L, Wu D, et al. The local cone and rod system function in early age-related macular degeneration. *Doc Ophthalmol*. 2004;109:1–8.
35. Parisi V, Tedeschi M, Gallinaro G, Varano M, Saviano S, Piermarocchi S. CARMIS Study Group. Carotenoids and antioxidants in age-related maculopathy Italian study: multifocal electroretinogram modifications after 1 year. *Ophthalmology*. 2008;115:324–333.
36. González-García E, Vilela C, Navea A, Arnal E, Muriach M, Romero FJ. Electrophysiological and clinical tests in dry age-related macular degeneration follow-up: differences between mfERG and OCT. *Doc Ophthalmol*. 2016;133:31–39.
37. Garcia-Garcia JG, Ruiz-Moreno JM, Holm K, Andreasson S, Lövestam-Adrian M. Macular dysfunction in drusen maculopathy assessed with multifocal electroretinogram and optical coherence tomography. *Clin Ophthalmol*. 2013;7:1303–1309.
38. Gin TJ, Luu CD, Guymer RH. Central retinal function as measured by the multifocal electroretinogram and flicker perimetry in early age-related macular degeneration. *Invest Ophthalmol Vis Sci*. 2011;52:9267–9274.
39. Yavas GF, Küsbeci T, Inan UU. Multifocal electroretinography in subjects with age-related macular degeneration. *Doc Ophthalmol*. 2014;129:167–175.
40. Hood DC, Bach M, Brigell M, et al. ISCEV standard for clinical multifocal electroretinography (2011 edition). *Doc Ophthalmol*. 2012;124:1–13.
41. Parisi V, Ziccardi L, Stifano G, Montrone L, Gallinaro G, Falsini B. Impact of regional retinal responses on cortical visually evoked responses: multifocal ERGs and VEPs in the retinitis pigmentosa model. *Clin Neurophysiol*. 2010;121:3850–3855.
42. Parisi V, Ziccardi L, Centofanti M, et al. Macular function in eyes with open-angle glaucoma evaluated by multifocal electroretinogram. *Invest Ophthalmol Vis Sci*. 2012;53:6973–6980.
43. Parravano M, Parisi V, Ziccardi L, et al. Single-session photodynamic therapy combined with intravitreal ranibizumab for neovascular age-related macular degeneration: a comprehensive functional retinal assessment. *Doc Ophthalmol*. 2013;127:217–225.
44. Sonoda S, Sakamoto T, Yamashita T, et al. Choroidal structure in normal eyes and after photodynamic therapy determined by binarization of optical coherence tomographic images. *Invest Ophthalmol Vis Sci*. 2014;55:3893–3899.
45. Corvi F, Pellegrini M, Erba S, Cozzi M, Staurenghi G, Giani A. Reproducibility of vessel density, fractal dimension, and foveal avascular zone using 7 different optical coherence tomography angiography devices. *Am J Ophthalmol*. 2018;186:25–31.
46. Curcio CA, Medeiros NE, Millican CL. Photoreceptor loss in age-related macular degeneration. *Invest Ophthalmol Vis Sci*. 1996;37:1236–1249.
47. Zarbin MA, Casaroli-Marano RP, Rosenfeld PJ. Age-related macular degeneration: clinical findings, histopathology and imaging techniques. *Dev Ophthalmol*. 2014;53:1–32.
48. Kennedy CJ, Rakoczy PE, Constable IJ. Lipofuscin of the retinal pigment epithelium: a review. *Eye (Lond)*. 1995;9:763–771.
49. Curcio CA. Photoreceptor topography in ageing and age-related maculopathy. *Eye (Lond)*. 2001;15:376–383.
50. Bok D. Retinal photoreceptor-pigment epithelium interactions: Friedenwald lecture. *Invest Ophthalmol Vis Sci*. 1985;26:1659–1694.
51. Green WR, Enger C. Age-related macular degeneration histopathologic studies: the 1992 Lorenz E. Zimmerman lecture. *Ophthalmology*. 1993;100:1519–1535.
52. Green WR. Histopathology of age-related macular degeneration. *Mol Vis*. 1999;3:5–27.
53. Nivison-Smith L, Wang H, Assaad N, Kalloniatis M. Retinal thickness changes throughout the natural history of drusen in age-related macular degeneration. *Optom Vis Sci*. 2018;95:648–665.
54. Nittala MG, Hogg RE, Luo Y, et al. Changes in retinal layer thickness in the contralateral eye of patients with unilateral neovascular age-related macular degeneration. *Ophthalmol Retina*. 2019;3:112–121.
55. Sadigh S, Cideciyan AV, Sumaroka A, et al. Abnormal thickening as well as thinning of the photoreceptor layer in intermediate age-related macular degeneration. *Invest Ophthalmol Vis Sci*. 2013;54:1603–1612.
56. Borrelli E, Mastropasqua R, Senatore A, et al. Impact of choriocapillaris flow on multifocal electroretinography in intermediate age-related macular degeneration eyes. *Invest Ophthalmol Vis Sci*. 2018;59:AMD25–AMD30.

Investigative Ophthalmology & Visual Science

Downloaded from iovs.arvojournals.org on 04/24/2024